AUT Journal of Mechanical Engineering

AUT J. Mech. Eng., 4(4) (2020) 449-464
DOI: 10.22060/ajme.2020.16836.5836

Computational fluid dynamics modeling and multi-objective optimization of flat tubes partially filled with a porous layer using ANFIS, GMDH, and NSGA II approaches

E. Rezaei*, A. Abbassi

Department of Mechanical Engineering, Amirkabir University of Technology (Tehran Polytechnic), Tehran, Iran

ABSTRACT: In this work, the fluid flow in flat tubes armed with a porous layer is modeled and multi-objectively optimized utilizing computational fluid dynamics methods, Adaptive-network-based fuzzy inference system, grouped technique of data handling type artificial neural network, and non-dominated sorting genetic algorithm II. The variables design includes the tubes' two geometrical parameters, porous layer thickness ratio, tube flattening, porosity, entrance flow rate, and wall heat flux. The purposes are to minimize the pressure drop and to maximize the convection heat transfer coefficient. Initially, utilizing computational fluid dynamics methods the problem is solved numerically in different flat tubes to calculate two objective parameters in tubes. Using numerical results of the preceding step, and are modeled through adaptive-network-based fuzzy inference system and grouped technique for handling the data. Then, Pareto-based multi-objective optimizing will be performed employing grouped technique of data handling model and non-dominated sorting genetic algorithm II. The results revealed that a better predicting is obtained by the adaptive-network-based fuzzy inference system model compared to the other approaches and the significant design information is included in the attained Pareto solution on flow parameters in flat tubes partly with porous insert. Based on the findings, the best configuring for the highest heat transfer and the least pressure loss is Hp= 0.75 *and* H=4mm.

Review History:
Received: Jul. 27, 2019
Revised: Dec. 20, 2019
Accepted: Jan. 26, 2020
Available Online: Nov. 25, 2020

Keywords:
Heat Transfer
Flat tubes
Porous medium
Modeling
Optimization

1- Introduction

Today, with the improvement of industries and utilization of equipment with higher efficiency and greater thermal energy production, it is necessary that the heat transferability of cooling equipment be more efficient. Therefore, traditional heat transfer methods will not meet future needs, and the necessity of new methods is feeling.

The use of a special type of flat tubes, which has less thermal resistance than conventional circular pipes, is a way to increment heat transfer in tubes. Another way for increasing the heat transfer is adding a porous medium to the tubes, which, by reducing the hydrodynamic boundary layer, causes the heat transfer increments. Combining the two methods of increasing the heat transfer and finding optimal flow conditions for making cooperation between pressure drop and heat transfer is the main subject of the current study. Numerous studies exist in the literature on forced convection in a porous tube filled partially and ducts.

Alazmi and Vafai [1] within a numerical research investigated 2 various constant heat flux boundary conditions with 7 sub-models. Moreover, the impacts of Darcy number, Reynolds number, porosity, inertia parameter, solid-to-fluid conductivity ratio particle diameter were analyzed. In a numerical research, Mohammad [2] studied the flow heat transfer improvement in a pipe and channel fully and partly occupied with porous medium. The influences of porous layer thickness and Darcy number investigated. Pavel and Mohamad [3] presented numerical and experimental investigations of the effect of metallic porous inserts in a pipe with uniform heat flux and the impacts of porous diameter, porosity, thermal conductivity, and Reynolds number on the pressure drop and heat transfer rate are assessed. The findings indicated that greater heat transfer rates can be obtained utilizing porous inserts causing a rational pressure drop.

Shokouhmand et al. [4, 5] assessed a channel's thermal performance and conducted a comparison with two configurations. They found that the porous insert's location significantly affects the channel's thermal behavior.

In the Local Thermal Equilibrium (LTE) model, the continuity of heat flux and temperature can be used as the interface boundary circumstances. Since the different temperatures for solid and fluid phases in porous media for Local Thermal Non-Equilibrium (LTNE) model, an extra thermal boundary condition is required at the interface. Three different interface models were presented for the first time by Yang and Vafai [6] for the heat flux bifurcation within a composite system under LTNE circumstances. They considered the restrictions of each model and obtained the Nusselt number for the relevant factors. Yang and Vafai in

*Corresponding author's email: ehsanrezaei@aut.ac.ir

another study [7] investigated an exact solution for 5 basic forms of thermal circumstances at the interface between a porous medium and a fluid under LTNE condition. Ming et al. [8] assessed numerically the laminar fully established flow in the tube occupied by porous medium and investigated the effect of Reynolds number and porous radius on the temperature and velocity profiles, flow resistance coefficient, Performance evaluation criteria (PEC) value, and Nusselt number.

Another method for heat transfer increment is to use flattened tubes rather than circular tubes. In comparison to the circular tubes, the flat tubes include a greater surface area to cross-sectional area ratio that is utilized to increment the compactness and improve the heat transfer. Vajjha et al. [9] numerically assessed nanofluid flow in an automobile radiator's single flat tube. They utilized the convection heat transfer coefficient for the wall boundary condition and ultimately provided the association for the friction factor and local Nusselt number of the automobile flat tube. Razi et al. [10] took into account pressure drop and heat transfer of CuO–oil nanofluid empirically in different flat tubes and lastly provided associations for nanofluid flow's pressure drop and Nusselt number in horizontal flat tubes. A nanofluid flow was simulated by Abbassi and Safikhani [11] numerically in various flat tubes possessing constant heat flux and assessed the impacts of tube flattening on the heat transfer and fluid dynamic. Safikhani et al. in another research [12] optimized nanofluid flow in flat tubes utilizing Computational fluid dynamic (CFD), Genetic algorithm, and Artificial Neural Network (ANN). The design variables included internal height, flat tube, heat flux, volumetric flow rate, nanoparticles volume fraction, and nanoparticles' diameter and the final objective was to increment concurrently the heat transfer coefficient and to decrease the pressure drop in flat tubes.

Recently research was also concentrated on practical tube applications in terms of developing both soft computing fields such as computational intelligence and CFD. The Adaptive-Network-Based Fuzzy Inference System (ANFIS) [13] is one of the leading artificial neural networks for predicting outcomes in some engineering problems. For example, the ANFIS technique was utilized to predict the energy systems' performance like ground-coupled heat pump systems [14-16], solar systems [17] thermal energy storage [18], refrigeration systems [19-22], modeling the performance in heat exchangers [23-28] Heating, ventilation, and air conditioning (HVAC) systems [29]. ANN and ANFIS were used for predicting the natural convection in a triangular closed system by Varol et al. [24]. It was observed that the ANFIS process yields more significant value to the actual one compared to ANN. Rezaei et al. [27] utilized ANFIS for predicting the free convection in a partitioned cavity containing an adiabatic partition. Experimentally, the training data were attained to optimize the ANFIS structure and for the best ANFIS structure, moreover, the mean relative errors of the test and train data were obtained as 1.73% and 0.05%, respectively. In the case of heat transfer in tubes, Kumar and Das Swain [30] researched the applicability of ANFIS for modeling the flow boiling heat transfer over a tube bundle. The mass flux, row height, and heat flux are investigated as the input and the heat transfer coefficient as output. The model predicted the experimental heat transfer coefficient within an error of ±5%. Tahseen et al. [28] used the ANFIS to predict the pressure drop and heat transfer for in-line flat-tube configuration in a crossflow. The mean relative error for pressure drop and average Nusselt number were obtained less than 2.97% and 1.9%, respectively. Hasiloglu et al. [31] studied is the usefulness of ANFIS to predict transient heat transfer of circular duct flow with varying inlet temperature. The findings indicate that the ANFIS can be utilized to model the transient heat transfer within ducts. Mehrabi et al. [32] investigated the ANFIS to model the fluid flow and heat transfer features of helicoidally double-pipe heat exchangers using some experimental data for testing and training the data. The outcomes showed that the proposed modeling by ANFIS was effective and reliable.

Normally, incrementing the quantity of heat transfer results in an increased pressure drop. Hence, an arbitrary configuration with the least pressure loss and highest heat transfer was obtained by a multi-objective enhancement. A significant share of research has been devoted to heat exchangers. The ultimate goal in optimizing each heat exchanger is to maximize heat exchange while minimizing the pressure drop of fluids. By doing so, the initial and operational costs of these exchangers can be reduced and a small size of heat exchangers could be used. Wang et al. [33] provided a kind of shell-and-tube heat exchangers with fold baffles. The second-order polynomial response surface method and multi-objective genetic algorithm were adopted. A group of Pareto-optimal points was achieved, and a good consistency was found by the optimizing results with CFD simulation data containing the relative deviation of less than ±3%. The experimental associations of the friction coefficient and Nusselt number were acquired with the adjusted coefficient of 0.999 and 0.943, respectively. Liu et al. [34] developed CFD simulation and multi-objective optimizing a plate-fin heat exchanger for the hydraulic retarder. The Non-dominated Sorting Genetic Algorithm II (NSGA-II) was employed. This research was only concentrated on improving the heat transfer behavior and the other parameter such as cost, maintenance, etc. was not considered. In a numerical simulation, Zheng et al. [35] assessed the thermal-hydraulic performance of a heat exchanger tube with vortex rod inserts. For achieving the best outline of the highest heat transfer improvement with the least pressure drop, multi-objective optimization was applied and the optimal Pareto front was obtained. Wang et al. [36] by combining multi-objective genetic algorithm and genetic aggregation response surface investigated the impacts of configuration parameters of the heat exchanger between the tube and shell. The average heat transfer coefficient of the enhanced configuration is improved by 2.93% while reducing the average pressure drop by 40.27%.

In this research, by considering geometrical elements like the porous layer thickness ratio, tube flattening, porosity of porous layer, wall heat, and entrance flow rate a multi-objective enhancement was performed for maximization of

the heat transfer and minimization of the pressure drop in a flat tube. To do this, some flat-tube geometries have been numerically solved by the use of the CFD approach. The findings were utilized to acquire the polynomials of the Group Method of Data Handling (GMDH) type neural network. The GMDH neural network as the heuristic self-organization technique models complex systems and is mostly used to convert discrete data to incessant functions [37]. Using the regression method, this technique creates quadratic polynomial functions within a feed-forward network. The method was used by many researchers [12, 38-41]. This neural network's outputs are applied as inputs for optimizing NSGA-II multi-objectively. NSGA II algorithm is one of the most comprehensive and the best multi-objective optimizing algorithms utilized in this study as well. Deb et al. [42] initially introduced this algorithm and recently it is utilized in different engineering-related applications [38-39, 43]. A set of optimal solutions, called Pareto solutions is obtained using multi-objective optimizing.

In the current study, the simultaneous impacts of a porous layer and flattening the tube on pressure drop and flow heat transfer are investigated using the CFD technique. The tube partly was filled with a porous medium while the wall is exposed to the constant wall heat flux. The flow field in the different flattened tube with The Darcy–Brinkman–Forchheimer model is utilized. ANFIS model was employed for accurately predicting the pressure drop and heat transfer in the tube. For training the ANFIS model, we used CFD data from the previous section. ANFIS model developed with five input parameters and two outputs for predicting the pressure drop and Nusselt number. Then, using genetically enhanced GMDH-type neural networks, polynomial models are acquired. The attained simple polynomial models are then employed in a Pareto-based multi-objective optimizing method for finding the best possible combinations of p and, namely as the Pareto front. The GMDH findings were compared to those of the ANFIS. In the optimizing procedure, the minimum friction factor and maximum heat transfer were treated as the multi-objective optimizing problem owing to the existence of two conflicting objectives. The tube flattening, the porous layer thickness ratio, porosity of porous layer, wall heat fluxes and entrance flow rate were design parameter variables. Some significant design principles are established by the equivalent variations of design variables, identified as the Pareto set.

2- Problem Statement

In this study, the thermal flow is taken into account within a horizontal flat tube with constant heat flux and partly full by a porous medium. The present simulations' geometry includes 5 horizontal flat tubes with various flattening and the same porous layers and perimeter (Fig. 1). The porous substance is put alongside the centerline of the tube. The same perimeter is a restriction found by the other researchers studying flat tubes [10, 11]. Table 1 compares some imperative geometrical parameters of flattened tubes. The fluid flow enters the tube with uniform and constant temperature and velocity.

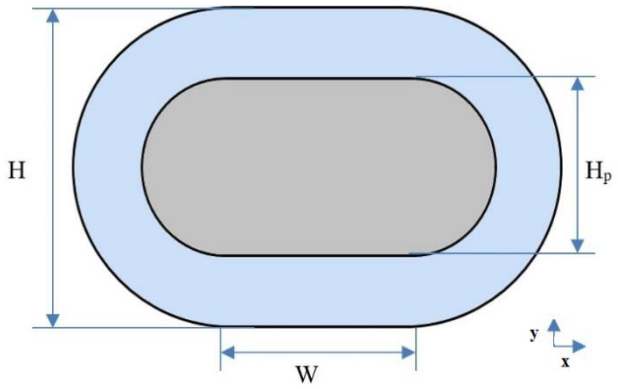

Fig. 1. Schematic of Flat tube with Porous layer

Table 1. Geometrical parameters of flattened tubes and porous layers

Flat tube No.	H (mm)	W (mm)	D_h
1	10	0	10
2	8	3.14	9.6
3	6	6.28	8.4
4	4	9.42	6.4
5	2	12.56	3.6
Porous Layer ratios No.	**H_p**		
1	0		
2	0.25H		
3	0.5H		
4	0.75H		
5	H		

It should be stated that considering the different tubes' hydraulic diameters, hence, the findings should not be expressed in the non-dimensional form. Thus, non-dimensional parameters like Nu, C_f, Re, H_p/D_h, and H/D_h are not used rather their dimensional elements like h, Q_{in}, q_w, H and H_p are utilized. In this work, to compare the behaviors of various flat tubes, the peripherally averaged values of factors like wall shear stress and heat transfer coefficient are compared.

2.1. Governing equations and boundary conditions

The thermos-physical features of fluid and solid phases are supposed to be constant. Steady, incompressible and laminar regime was considered and natural convection, gravitational effects and radiative heat transfer are ignored. The Darcy-Brinkman model is used for modeling the momentum equation in porous substance, isotropic and homogeneous characteristics are supposed for the porous structure, LTNE model, Yang and Vafaei [6] between the fluid and solid phases in the porous medium are considered.

Under these conditions the governing equations are expressed [44]. These yields, continuity

$$\nabla.\vec{V} = 0 \tag{1}$$

momentum in the void region

$$\rho(\vec{V}.\nabla)\vec{V} = -\nabla P + \mu\nabla^2\vec{V} \tag{2}$$

momentum in the porous region based on the Brinkman-Forchheimer-extended Darcy equation

$$\frac{\rho}{\varepsilon}(\vec{V}.\nabla)\vec{V} = -\nabla P + \frac{\mu}{\varepsilon}\nabla^2\vec{V} - \frac{\mu}{K}\vec{V} - \frac{\rho F\varepsilon}{\sqrt{K}}\left|\vec{V}\right|\vec{V} \tag{3}$$

where, F is the inertial coefficient, ε is the porosity and K is the permeability of the porous media. K can be written as [45]:

$$K = \frac{\varepsilon^3 d_p^2}{150(1-\varepsilon)^2} \tag{4}$$

where d_p is particle diameter. The inertial coefficient is expressed as follows:

$$F = \frac{1.75}{\sqrt{150}\varepsilon^{3/2}} \tag{5}$$

fluid phase of energy equation in the clear region:

$$\vec{V}.\nabla T = \alpha\nabla^2 T \tag{6}$$

fluid phase of energy equation in the porous region:

$$\left(\rho c\right)_f \vec{V}.\nabla T_f = \nabla.(k_{fe}\nabla T_f) + h_{sf}a_{sf}(T_s - T_f) \tag{7}$$

solid phase of energy equation in the porous region:

$$0 = \nabla.(k_{se}\nabla T_s) - h_{sf}a_{sf}(T_s - T_f) \tag{8}$$

The subscripts 'f' and 's' denote the fluid and solid phases, respectively. T is temperature, V is the fluid velocity and P is the pressure. ρ_f, μ and C_p are respectively density, viscosity and specific heat capacity of the fluid. The effective conductivities of the porous media and the fluid are respectively k_{se} and k_{fe}. These two geometrical functions of the porous media are expressed as follows:

$$k_{se} = (1-\varepsilon)k_s$$
$$k_{fe} = \varepsilon k_f \tag{9}$$

The specific surface area in the energy equations declared as:

$$a_{sf} = \frac{6(1-\varepsilon)}{d_p} \tag{10}$$

The fluid-to-solid heat transfer coefficient is expressed as:

$$h_{sf} = k_f[2 + 1.1\,\mathrm{Pr}^{1/3}\,\mathrm{Re}_p^{0.6}]/d_p \tag{11}$$

Pr is the Prandtl number and Re_p is Reynolds number of particle:

$$\mathrm{Re}_p = \rho V_i d_p/\mu \tag{12}$$

At the entrance, Z = 0, T = T_i and V = V_i. The gradients of V in X and Y direction are zero. In summary, the boundary conditions are:

At Z=0:

$$\vec{V}_z = \vec{V}_i$$
$$\vec{V}_x = \vec{V}_y = 0 \tag{13}$$
$$T = T_i$$

At wall:

$$\vec{V} = 0$$
$$q''_w = -k\left.\frac{\partial T}{\partial n}\right|_w \tag{14}$$

At the interface between the fluid and porous media:

$$\vec{V}_x\big|_- = \vec{V}_x\big|_+ \quad , \quad \vec{V}_y\big|_- = \vec{V}_y\big|_+$$
$$T_x\big|_- = T_x\big|_+ \quad , \quad T_y\big|_- = T_y\big|_+ \tag{15}$$

The conditions for heat transfer at the boundary between the fluid and porous medium expressed as:

$$k_{se}\left.\frac{\partial T_s}{\partial n}\right|_- = k_{fe}\left.\frac{\partial T_f}{\partial n}\right|_- = \frac{1}{2}q_{interface} \tag{16}$$

where $q_{interface}$ is the heat flux at the interface of solid and fluid. The shear stress condition at the interface is:

$$\mu_{eff}\left.\frac{\partial V_f}{\partial n}\right|_- = \mu_f\left.\frac{\partial V_f}{\partial n}\right|_+ = 0 \tag{17}$$

Based on the hydraulic diameter and the velocity in the range of laminar flow regime, exit conditions can be considered fully developed:

At Z=L

$$\frac{\partial V_x}{\partial z} = \frac{\partial V_y}{\partial z} = 0$$
$$\frac{\partial T}{\partial z}cte = \frac{P}{A}\frac{q''}{\rho UC_p} \tag{18}$$

3- Numerical Simulation

The numerical simulation is carried out utilizing the

Table 2. Detailed information of simulations

Solver	Pressure Based	**Fluid**	
Velocity formulation	Relative	Water	
Viscous	Laminar/Standard K-ε	Density (kg/m^3)	998
Properties	Piecewise-Polynomial	Heat capacity (J/kg K)	4182
Porous Zone	Non-Equilibrium	Thermal conductivity (W/m K)	0.6
Solution Method		**Porous**	
Scheme	SIMPLE	Aluminium	
Spatial Discretization		Density (kg/m^3)	2719
Gradient	Least Squares Cell-Based	Heat capacity (J/kg K)	871
Pressure, Momentum, Energy	Second-order Upwind	Thermal conductivity (W/m K)	202
Under-Relaxation Factors		Wall heat flux (W/m^2)	2000-10000
Pressure	0.3	Flow rate (m^3/hr)	0.0024-0.0218
Momentum	0.7	Inlet temperature (K)	300
Density, Body Force, Energy	1		

finite volume technique. The governing equations were transformed into algebraic equations through a control-volume-based method so that these equations can be solved numerically. The second-order upwind outline is utilized for the space discretizing of the convective terms in energy and momentum equations, and to couple the velocity and pressure, the Semi-Implicit technique for Pressure Linked Equations (SIMPLE) algorithm is utilized. A second-order scheme is also used for the space discretizing of pressure. For all solved variables' normalized residuals, the convergence criteria are limited to be less than 10^{-6}. The sub-relaxation iteration technique is employed for CFD simulations, to guarantee the convergence of the simulation. Furthermore, the detailed data of simulations are provided in Table 2.

3.1. Grid size selection

For verifying the grid independence and for arriving at the least number of factors yielding precise computational outcomes, the grid independency test is performed. According to Fig. 2, four-line sections were taken into account by *G1*, *G2*, *G3* and *G4*, respectively indicating the number of points alongside the flat part's width, the flat section's length, the semi circles' perimeter and alongside the tube's length. Here, 4 different grid systems are examined including mesh I: 30×40×350×50, mesh II: 50×60×400×40, mesh III: 50×60×450×70 and mesh IV: 60×70×500×80. The 4 meshes were examined through comparison of the axial velocity, heat transfer and temperature coefficient for laminar flow in the flat tube with H = 6 mm occupied with porous media with H_p=0.5 (Fig. 3). The temperature and velocity in x and y directions attained from mesh I, do not accommodate to the findings from the other 3 kinds of meshes. The highest variation of V in Z direction between the Mesh II and other meshes of I, III and VI are 0.03%, 0.01% and 0.01% respectively. The greatest difference of h between Mesh II and other meshes are 15.25%, 3.77% and 3.33% respectively for Mesh I, III and VI. Consequently, mesh II is selected and all calculations were performed with this grid. The total number of hexagonal nodes was 2,621,925. Fig. 4 represents the created mesh for a flat tube utilizing the stated grids. Based on this mesh grid, the

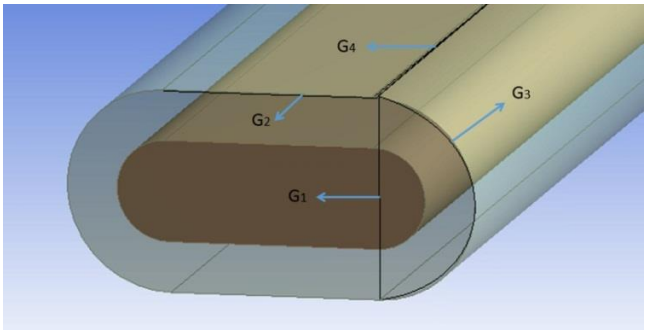

Fig. 2. Line segments used for Grid size selection

temperature difference between fluid and solid phase at the end of the flat tube cross-section and also pressure drop along the tube illustrated in the Figs. 5 and 6.

For checking the solution's validity, without any former study regarding flat tubes with a porous layer, two comparisons were examined between the findings obtained by the existing program and the findings of the other scholars. At first, the circular tubes are compared with a porous layer inserted in the selected tube's core. Fig. 7 compared the solution attained by the existing and the numerical solution of Karimi and Mahmoudi [45] (for the Nusselt number of laminar flow in a tube partly occupied with porous substance). Based on the comparison, it is showed that the highest deviation and the average deviation found by Karimi and Mahmoudi [45] for the average Nusselt number are 3.1% and 2.9 % respectively. Within the second comparison, flat tubes in the absence of porous layer investigated by Abbassi and Safikhani [11], are compared and provided in Fig. 8. Comparing average heat transfer coefficient versus flattening indicates that the highest deviation and the average deviation from the data of Abbassi and Safikhani [11] for local heat transfer coefficient are 2.8% and 1.9 % respectively. Hence, it is found that the regarded computational model exists for solving the flow and laminar heat transfer problem for a flat tube with a porous insert.

4- Modeling of *h* and *dP*

In this section, the discrete points obtained from CFD

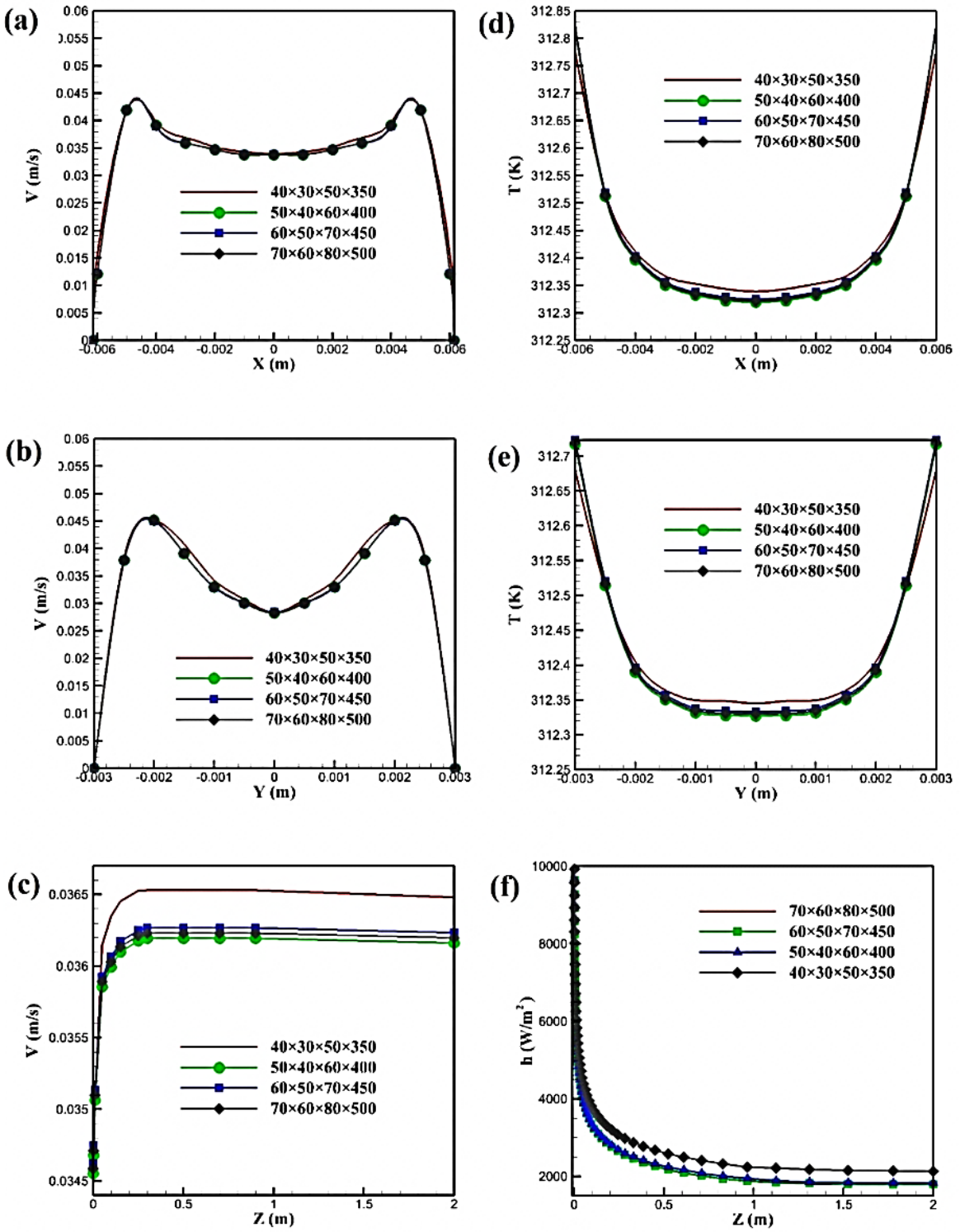

Fig. 3. Grid independency test for H = 6 mm, (a) velocity distribution in x direction, (b) velocity distribution in y direction, (c) velocity distribution in z direction, (d) temperature distribution in x direction, (e) temperature distribution in y direction and (f) local heat transfer coefficient distribution in z direction.

solutions were used in multi-objective optimization by neural networks are presented. In other words, the neural network will be able to receive design variables as inputs and calculate pressure drop and heat transfer coefficient as outputs.

4.1. Adaptive neuro-fuzzy inference system

The artificial neural network is a calculating instrument utilized to examine the data and to make a model by these data. ANFIS [46, 47] is an adaptive network making it possible

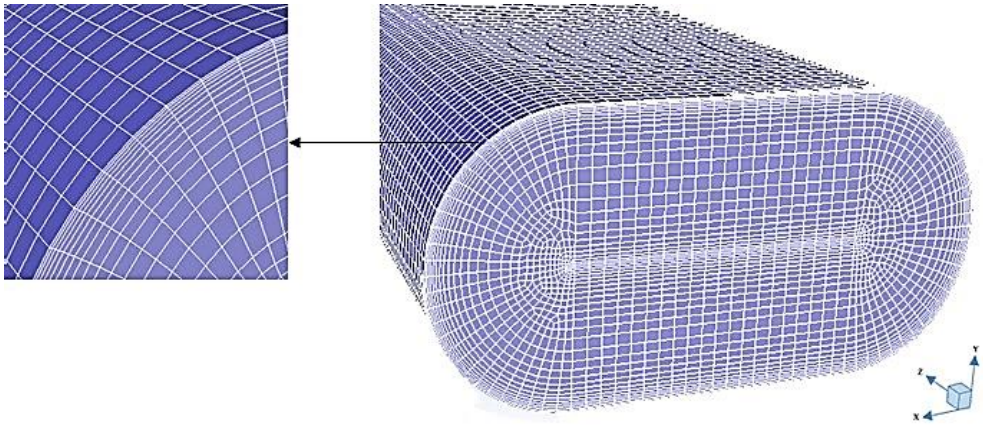

Fig. 4. Grid layout used in the present numerical computation

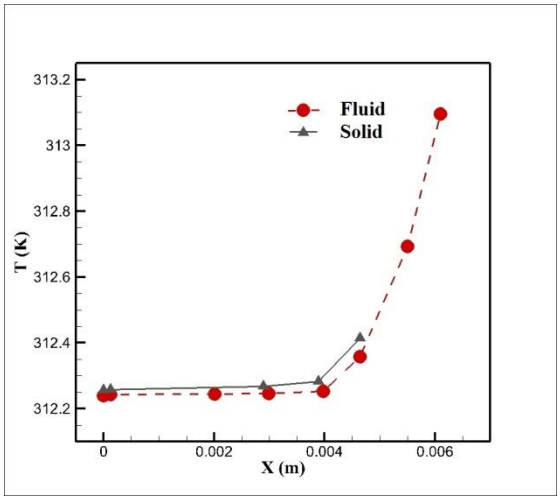

Fig. 5. Fluid and solid temperature profiles at the exit cross-section

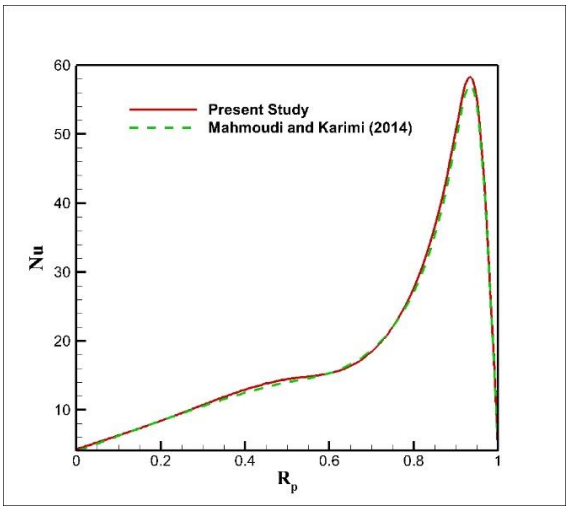

Fig. 7. Comparison between the present study and Mahmoudi and Karimi [45]

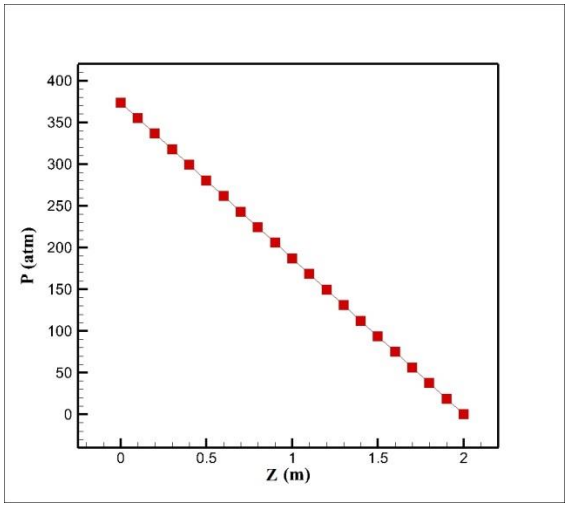

Fig. 6. Pressure drop distribution along the flat tube

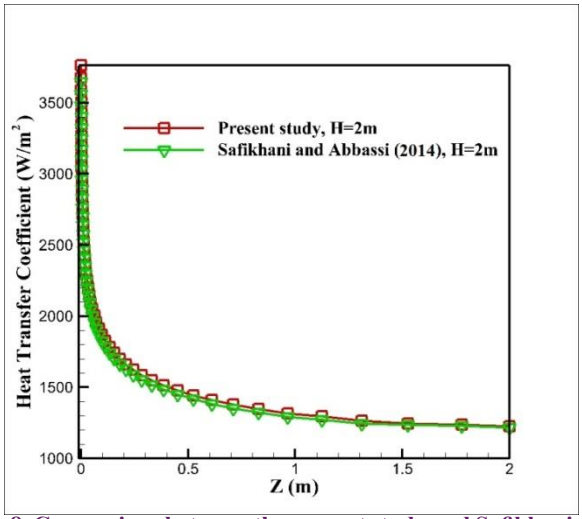

Fig. 8. Comparison between the present study and Safikhani and Abbassi [11]

to implement the neural network topology, along with fuzzy logic [48]. By combining these two systems, a proper result may be quantitatively and qualitatively achieved including either calculative capabilities or fuzzy intellect of the neural network and using the advantages of both methods. The

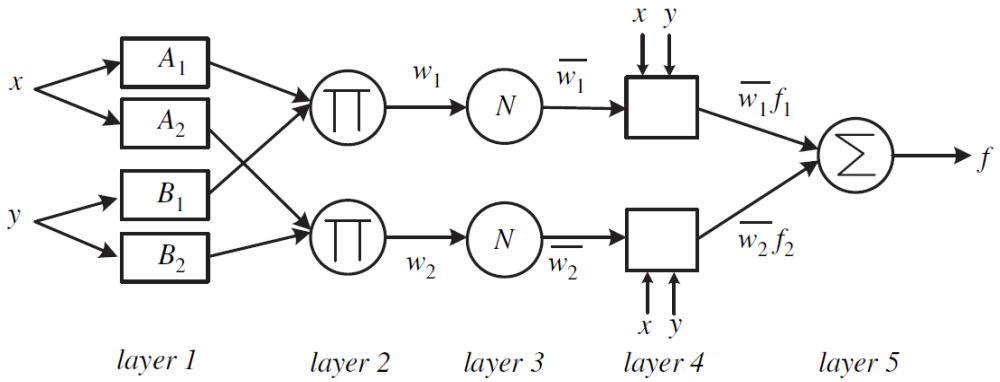

Fig. 9. ANFIS architecture based on Takagi–Sugeno.

ANFIS's main target is to discover a model able to model inputs with the outputs accurately. We run a Takagi–Sugeno fuzzy inference system containing an architecture with five layers. Fig. 9 shows the diagram of this architecture and the suggested ANFIS model. For making simple, supposing that the fuzzy inference system includes two inputs of x and y and an output f which related to the following rules:

Rule 1 If (x is A_1) and (y is B_1) then $f_1=p_1x+q_1y+r_1$

Rule 2 If (x is A_2) and (y is B_2) then $f_2=p_2x+q_2y+r_2$

in which A_i, B_i and f_i are fuzzy sets and output of the system respectively. p_i, q_i and r_i are designing factors attained over the learning procedure. Each layer's output in the ANFIS network consider as O_{ij} (ith node output in jth layer) so the functions of the different layers of this network explain as:

Layer 1

In this layer, each node is equivalent to a node's output and fuzzy set in the respective fuzzy set corresponding to the input variable membership grade. Each node's parameters define the membership function form in the fuzzy set described by a Gaussian function, so we will have:

$$\mu_A(x)=\frac{1}{1+\left|\frac{x-c_i}{a_i}\right|^{2bi}} \tag{19}$$

where a_i, b_i and c_i denote the premise factors.

Layer 2

In this layer, multiplying the values of each node's input signals by each other, a rule firing strength (wi) is calculated.

$$O_{2,i}=W_i=\mu_{Ai}(x)\mu_{Bi}(y) \quad i=1,2 \tag{20}$$

where μAi shows the membership grade of x in Ai fuzzy set and μBi represents the membership of y in the fuzzy set of Bi.

Layer 3

In this layer, each node approximates the ratio (w_i) of firing strength of the ith rule to the summation of all rules' firing strength. They normalize the firing strength of the former layer. Here, each node's output is:

$$O_{3,i}=W_i=W_i/W_1+W_2 \quad i=1,2 \tag{21}$$

This layer's outputs are known as normalized firing strengths.

Table 3. Optimal architecture and specification of the proposed ANFIS model.

Type	Takagi-Sugeno
Inputs	5
Outputs	2 (1 at a time)
Number of input membership function	10 for all inputs
Number of output membership function	8
Input membership function Types	Gaussian
Output membership function Types	Linear
Rules Weight	1
Number of fuzzy rules	14
Number of epochs	100

Layer 4

In this layer that name is rule layer, each node's output is the product of the formerly obtained relative firing strength of the ith rule by first-order polynomial Sugeno fuzzy rule:

$$O_{4,i}=W_if_i=W_i(p_ix+q_iy+r_i) \quad i=1,2 \tag{22}$$

where p_i, q_i and r_i show design elements. This layer's output is the compression of a linear mixture of inputs multiplied by the normalized firing strength W.

Layer 5

Layer 5, this layer is the network's last layer and includes one node and adds up all node's inputs. It calculates the total output as the sum of all incoming signals from layer 4:

$$O_{5,i}=\sum_{i=1}^{2}W_if_i=\frac{\sum_{i=1}^{2}W_if_i}{\sum_{i=1}^{2}W_i} \tag{23}$$

The ANFIS output is calculated utilizing the resultant parameters in the forward pass. For the adaption of premise parameters, the output error is used through a standard back-propagation algorithm. It was confirmed that this hybrid algorithm is greatly effective in training the ANFIS. Table 3 represents the ANFIS's parameters utilized in this work. More details about the ANFIS algorithm can be found in references [13, 14]. In general, the networks' performances are appraised utilizing the statistical coefficient of correlation coefficients

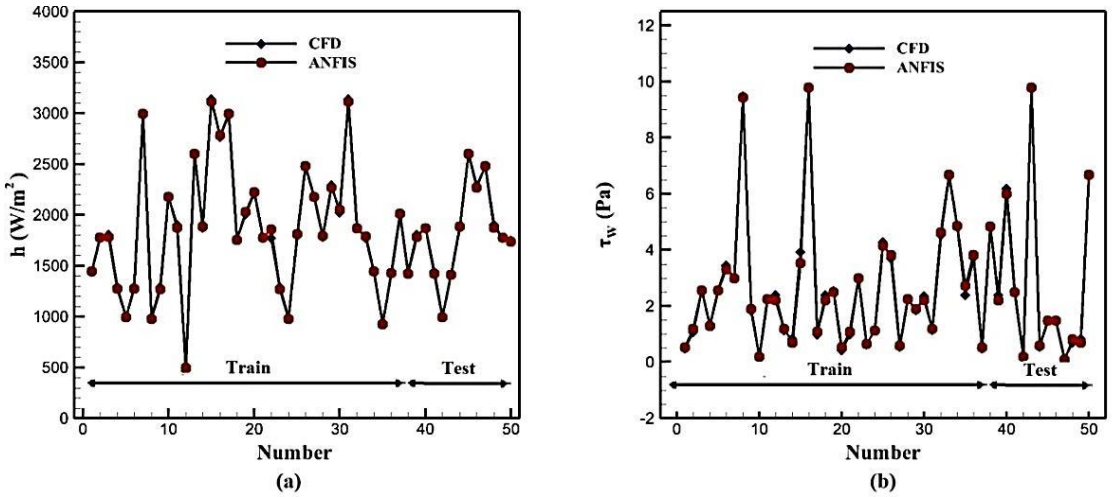

Fig. 10. Comparison of (a) *h* and (b) τ_w predicted by ANFIS and simulated by CFD

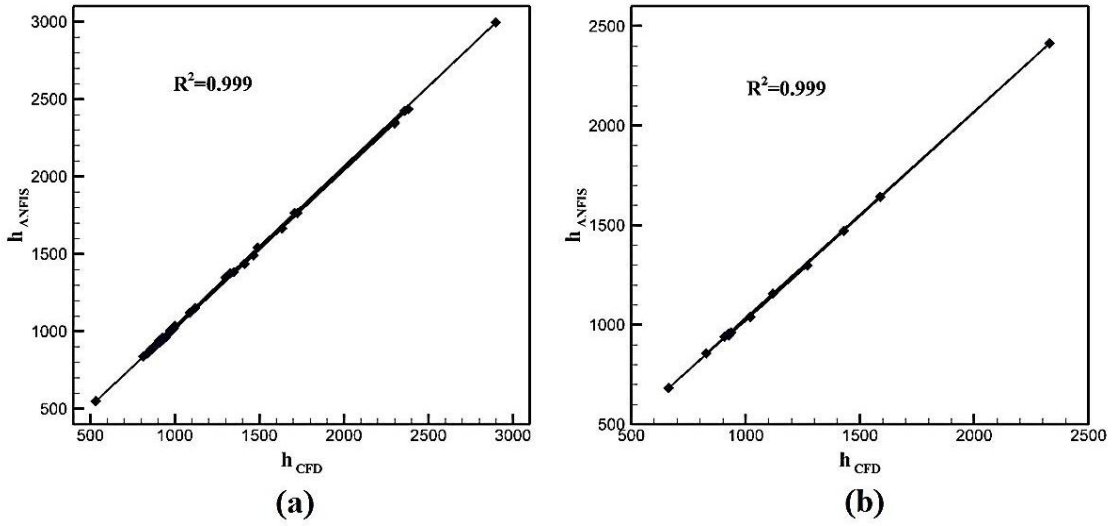

Fig. 11. The R^2 squared comparison of the numerical and predicted values of average heat transfer coefficient using ANFIS models for (a) training data and (b) testing data.

(R^2), Mean Relative Error (MRE), and Root-Mean-Square Error (RMSE) values, which are determined by the following expressions:

$$R^2 = 1 - \frac{(\sum_{i=1}^{N}(Q_i - P_i)^2)}{(\sum_{i=1}^{N} P_i^2)}$$

$$RE\% = \left|\frac{Q_i - P_i}{Q_i}\right| \times 100 \tag{24}$$

$$MRE\% = \frac{1}{N}\sum_{i=1}^{N}\left|\frac{Q_i - P_i}{Q_i}\right| \times 100$$

where Q_i shows the actual value, P_i represents the ANFIS output or foreseen value, n shows the number of output data.

The input parameters were tube flattening ranging from 2 to 10 mm, porous layer thickness ratio from 0 to 1, the porosity of porous layer ranging from 0.1 to 0.9, wall heat flux ranging from 2000 to 10000 (W/m²), and entrance flow rate ranging from 0.0024 to 0.0218 (m³/hr) were design parameter. The output parameters were convection heat transfer (h) and wall shear stress (τ_w). Due to the various hydraulic diameter of flat tubes, in this study, the wall shear stress was utilized rather than pressure drop. These two factors are:

$$\Delta P = C_f \frac{8L}{D_h}\rho V^2 \tag{25}$$

$$C_f = \frac{1}{2}\frac{\tau_w}{\rho V^2} \tag{26}$$

where L represents length and D_h shows the hydraulic diameter of tube. Fifty sets of input parameters have been chosen by the use of Design of Using (DOE) technique

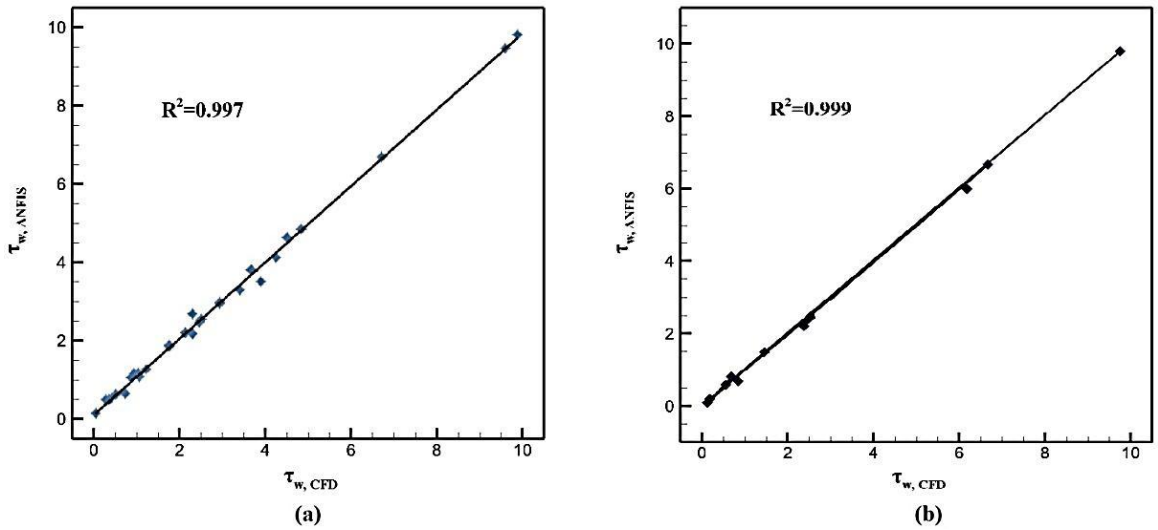

Fig. 12. The R^2 squared comparison of the numerical and predicted values of average wall shear stress using ANFIS models for (a) training data and (b) testing data.

to construct the models of ANFIS. In the present paper, Response Surface Methodology (RSM) as a sub technique of DOE [49], the number of input-output data are designed in GMDH modeling. Taking into account 5 design variables and 2 objective functions, a total number of 50 input-output CFD data is obtained.

To enhance the ANFIS model, around 75% of data are utilized to train and 25% to test the behavior. The ANFIS models for testing and training data for h and τ_w are provided in Fig. 10-12. It is obvious that comparing among there is a good consistency within the predicted and numerical values of heat transfer coefficient and pressure drop utilizing ANFIS model with more R-square value of higher than 0.999. Furthermore, the appropriate difference in error values between the test and train data set confirms the model's reliability. It is also seen that the greater relative error of the average Nusselt number was about 2.68% (for training) and 2.75% (for testing). Moreover, the mean relative error is ranged from 0.1-3%. The greater values of dimensionless pressure drop's relative error were about 3.08% (for testing) and 2.92% (for training) and the mean relative error is ranged within 2.71-2.57%.

4.2. GMDH

The group technique of data handling algorithm [37], originally introduced by Ivakhnenko is one of the widely used and most complete neural networks, also recognized by polynomial neural network. The main application of GMDH is function approximation, complex systems modeling, pattern recognition, and nonlinear regression. Dissimilar to the other usual kinds of ANN, the GMDH network is a self-organizer indicating no need for specifying the number of layers and neurons or the net and transfer functions since these factors are automatically determined. Besides, the GMDH model prepares a set of mathematical equations rather than ANN regular matrix structure, hence, the output is more practical.

In this technique, the neural network is created by connecting various pairs of neurons via a quadratic polynomial. The network attained from combined quadratic polynomials states the approximating function $\hat{f}$ and output $\hat{y}$ for a set of inputs $x = (x_1, x_2, \ldots, x_n)$ compared to the real output with the minimum error value. Thus, the real results for n inputs and one output expressed as:

$$y_i = f(x_{i1}, x_{i2}, ..., x_{in}) \tag{27}$$

Now, the purpose is to find a network able to forecast the output y for each value of input x of Eq. (27):

$$\hat{y}_i = \hat{f}(x_{i1}, x_{i2}, ..., x_{in}) \tag{28}$$

The considered network should be capable of minimizing the square of the error between the predicted and real values:

$$MSE = \frac{\sum_{i=1}^{N} (\hat{y}_i - y_1)^2}{N} \rightarrow \min \tag{29}$$

The general relation between the input x and output $\hat{y}$ is stated as Volterra functional series also recognized as Kolmogorov-Gabor polynomial:

$$\hat{y} = a_0 + \sum_{i=1}^{n} a_i x_i + \sum_{i=1}^{n} \sum_{j=1}^{n} a_{ij} x_i x_j + \sum_{i=1}^{n} \sum_{j=1}^{n} \sum_{k=1}^{n} a_{ijk} x_i x_j x_k \tag{30}$$

In this equation, a is the coefficients or weights that will be defined to minimize the mean square error for the neuron. More details regarding the GMDH neural network exist in [50, 51]. Now, based on the GMDH algorithm, the polynomials relating the objective functions h and τ_w to input variables in flat tubes equipped with porous layers are

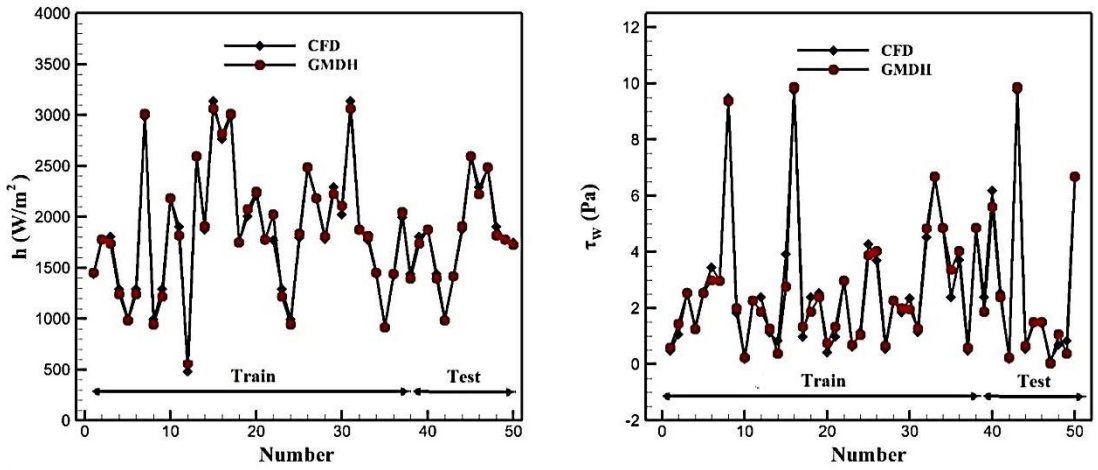

Fig. 13. Comparison of (a) *h* and (b) τ_w predicted by GMDH and simulated by CFD

Table 4. MRE and R^2 values of ANFIS and GMDH for prediction of *h* and τ_w

Method	*h* Training		*h* Testing		τ_w Training		τ_w Testing	
	MRE %	R^2	MRE %	R^2	MRE %	R^2	MRE %	R^2
ANFIS	2.683	0.999	2.757	0.999	2.929	0.999	3.088	0.998
GMDH	3.231	0.993	3.682	0.993	6.19	0.988	9.602	0.971

obtained. The polynomials functions associated with the h are obtained based on the GMDH algorithm, as:

$$Y_1 = 2245.06 - 63741.8\varepsilon \times Q$$

$$Y_2 = 697.288 + 3931.47 H_p - 2578.8 H_p^2$$

$$Y_3 = 3430.64 - 266.887 H$$

$$Y_4 = 3769.71 - 252.854 H - 864.635\varepsilon$$

$$Y_5 = 65.4845 + \left(5.17213\times10^{-4}\right) Y_2 \times Y_3$$

$$Y_6 = 529.514 + 0.732206 H_p \times Y_4 + \left(1.73014\times10^{-4}\right) Y_4^2$$

$$Y_7 = 70.767 + \left(5.15483\times10^{-4}\right) Y_2 \times Y_4$$

$$Y_8 = -219.489 + 1.35178\, Y_7 + 0.00619119\, Y_6 \times Y_7 - 0.00357408\, Y_7^2 - 0.00271756 Y_6^2$$

$$Y_9 = -26.2445 - 0.004218755 Y_5 \times Y_8 + 0.00208276\, Y_5^2 + 1.00254\, Y_8 + 0.00212022\, Y_8^2$$

$$\boldsymbol{h} = -36.9157 - \left(9.96073\times10^{-5}\right) \boldsymbol{Y}_1 \times \boldsymbol{Y}_9 + 1.20781\, \boldsymbol{Y}_9$$

Similarly, the GMDH polynomial functions for the wall shear stress in flat tubes are in the form of:

$$Y_1' = 4.803 - 0.666 H \times \varepsilon$$

$$Y_2' = 1.139 - 0.027 H^2 + 219.142 Q$$

$$Y_3' = 1.670 - 7.483 H_p \times \varepsilon + 9.502 H_p^2$$

$$Y_4' = 4.669 - 0.479 H - 5.254 H_p + 11.133 H_p^2$$

$$Y_5' = 0.004 + 0.135 Y_4'^2 + 0.143 Y_2'^2$$

$$Y_6' = 1.673 - 0.792\, Y_3' + 0.337\, Y_2' \times Y_3' + 0.139\, Y_3'^2 - 1.049\, Y_2' + 0.234\, Y_2'^2$$

$$Y_7' = 4.122 - 1.145\, H + 0.053\, H \times Y_6' + 0.079\, H^2 + 0.436\, Y_6' + 0.029\, Y_6'^2$$

$$Y_8' = -1.094 + 5.935\, H_p - 5.870 H_p^2 + 0.917\, Y_7' + 0.014\, Y_7'^2$$

$$Y_9' = -1.089 + 0.889 Y_1' - 0.158 Y_1'^2 + 0.989 Y_8'$$

$$\hat{\boldsymbol{o}}_{\boldsymbol{W}} = 0.050 - 0.071\, \boldsymbol{Y}_5' + 1.053\, \boldsymbol{Y}_9'$$

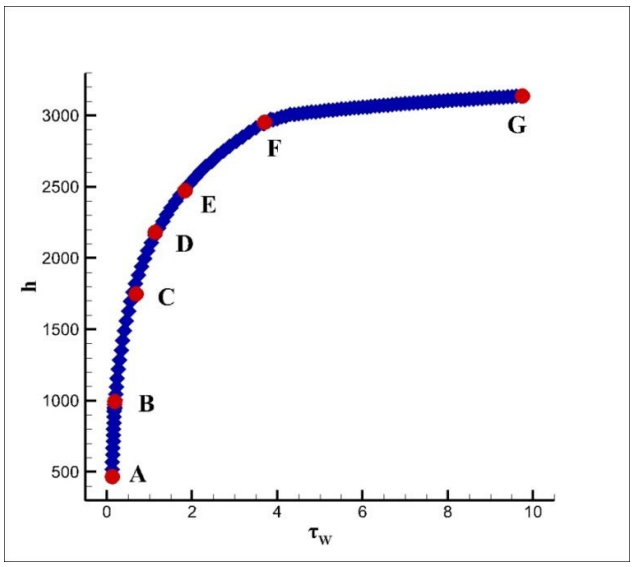

Fig. 14. Pareto optimal points for *h* and τ_w for optimal design points.

Fig. 13 presented the GMDH values for both the testing and training datasets of objective functions h and τ_w. All the training and testing data were randomly chosen. Comparing the findings attained from examining the neural network shows an acceptable consistency between the CFD and GMDH outcomes. The used neural network's satisfactory performance is indicated by this convergence. The attained GMDH models is utilized in the NSGA-II multi-objective optimizing technique.

For comparing the results predicted from the two established models, the quantity of MRE and R^2 for h and τ_w are given in the Table 4. According to this table, the established ANFIS models are more precise and generated more reliable estimations than the GMDH algorithm for h and τ_w prediction.

5- Multi-Objective Optimization Using GMDH Models

To survey the optimal behavior of flat tubes equipped with porous layer, the GMDH models attained in Section 4 are used now in a multi-objective optimizing technique utilizing NSGA II algorithms. Deb et al. [42] presented this algorithm as an improved NSGA. For maximizing the amount of heat transfer, it is vital to select appropriate values for design parameters. Nevertheless, the variation of these parameters values for enhancing the heat transfer normally increments the fluid pressure drop that is not desired. Hence, a point with the highest heat transfer and least pressure drop cannot be discovered. These two conflicting objectives h and τ_w need to be simultaneously enhanced based on the design variables: H, H_p, ε, Q and q''.

For solving this problem, rather than discovering one special state as the optimal state, a set of optimal states are attained. These groups of points named the Pareto optimal points or Pareto front are acquired through multi-objective enhancement. In multi-objective optimization problems, Pareto optimal points are a set of solutions that are better than other solutions and non-dominated to each other. Therefore, a change in design variables in such a Pareto front could not result in improving all objectives simultaneously and this change will result in a decrease of at least one objective. In all runs population size, mutation probability (Pm) and crossover probability (Pc) have been chosen as 60, 0.07, and 0.7, respectively.

The two-objective optimizing conducted in this work can be briefly explained as:

$$maximize \;\; h = f_1(H, H_p, \varepsilon, Q, q'')$$

$$minimize \;\; \tau_w = f_2(H, H_p, \varepsilon, Q, q'')$$

$$Subject\ to \; 2\text{mm} \le H \le 10\,\text{mm}$$

$$0 \le H_p \le 1$$

$$0.1 \le \varepsilon \le 0.9$$

$$0.0024\text{m3/h} \le Q \le 0.0218\text{m3/h}$$

$$2000 \le q'' \le 10000\,\text{W/m}^2$$

Fig. 14 reveals the obtained optimal design points as a Pareto front of those two objective functions. Four optimal design points, designated by A, B, C, D, E, F and G can be seen in this Figure, for which the equivalent design variables and objective functions were provided in Table 5. It is obvious that all the optimal points in Pareto front have no dominancy to each other, meaning that no objective function can be better without worsening at least another objective function and there is not two points, in which an objective function is the same and the other one is different.

Fig. 14 represents the design points A and G exhibiting the best pressure drop and the best heat transfer, respectively. In point G the heat transfer is maximum, though, it should be stated that under these conditions the pressure loss is also the highest. On the other hand, in point A both pressure loss and heat transfer are minimum. Moreover, the other points, B and F from Fig. 14 known as the breakpoints.

The design point, B shows important optimum design concepts. This point compared with point A indicates about 51% increases in τ_w and h. Similarly, point F compare with point G, h increments slightly (almost 24.1%), however, τ_w is enhanced by a greater value (almost 102.3%). In general, it is a desire to find out optimum design points compromising both objective functions. To detect that point, the mapping method was utilized [39]. Hence, first, the value of τ_w function is reversed (since the least value of this objective is desirable). The reversed τ_w and Nu functions of all non-dominated points are then mapped into interval 0 and 1, and calculate the norm of these functions. Utilizing the summation of mapped values, the trade-off point (point F) is the least sum of those values satisfying both objective functions of pressure loss and heat transfer.

For a useful comparing, the optimum data received from the Pareto front are compared and Figured accompanied by the present numerical data. Fig. 15 indicates the overlap of the

Table 5. Pareto corresponding design variables and objective functions

Point	H(mm)	H_p	ε	Q(m3/h)	q(W/m^2)	h	τ_w	Norm Value
A	6	0	0.5	0.0122	6000	466.63	0.126	1
B	8	0.25	0.7	0.0073	4000	993.1	0.185	1.187
C	6	0.5	0.5	0.0025	6000	1748	0.686	1.421
D	4	0.25	0.3	0.0073	4000	2180	1.135	1.535
E	4	0.75	0.7	0.0073	4000	2474.1	1.837	1.57
F	***4***	***0.75***	***0.3***	***0.0073***	***4000***	***2983.1***	***3.703***	***1.573***
G	4	0.75	0.3	0.017	8000	3137.9	9.751	1

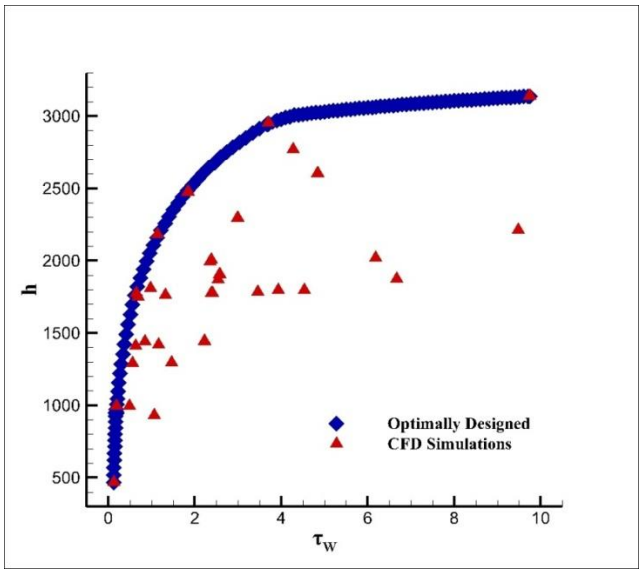

Fig. 15. Overlap graph of the obtained optimal Pareto front with the CFD simulation data

Pareto front and the related numerical data. The Figure shows that the Pareto front has identified the best boundary of the CFD data very precisely based on the minimum pressure drop and the maximum heat transfer coefficient confirming the validity of the multi-objective optimizing method provided in the present work.

6- Conclusions

In this work, modeling and multi-objective optimizing the parameters of flow in horizontal flat tubes equipped with porous insert were successfully performed through the combination of ANFIS, CFD, NSGAII and GMDH algorithm. The design variables were H, H_p, ε, Q and q″ and the essential target was to enhance concurrently the heat transfer coefficient and decrease the pressure drop in flat tubes. Initially, CFD methods were utilized for solving the flow in several flat tubes. Followed by validation of the findings, the CFD data in this phase were utilized to model the objective functions h and τ_w by ANFIS and GMDH type ANN. In ANFIS model, all the training and testing data have been selected randomly and about 75% of data are employed to train and 25% to test the performance. By utilization of various statistical parameters, the high accurateness of GMDH polynomials was represented. Ultimately, these polynomials were utilized for the multi-objective optimizing the parameters in flat tubes partially with porous media and the derivation of the Pareto front by the use of NSGAII algorithm. The Pareto front included significant design information concerning the flat tubes and porous layer, which could not be attained except for the combination of CFD, GMDH, and the multi-objective optimizing technique. This study can be concluded as:

1. The excellent adaption between the predicted heat transfer coefficient and the numerical results indicates that ANFIS is a reliable technique to model and predict the results owing to its high correctness.

2. The GMDH model presents simple mathematical equations without requiring a complicated numerical model. In other words, this model helped us in converting numerical outcomes to algebraic equations precisely.

3. The results indicated that the ANFIS Model is more precise than the GMDH Network. MRE% for training data of ANFIS and GMDH models are 2.68 and 3.23 and for testing data are 2.75 and 3.68 for heat transfer coefficient and training data of ANFIS and GMDH for wall shear stress are 2.92 and 6.19 and for testing data are 3.08 and 9.60.

4. In Pareto front, four numbers of distinguished points were specified including the point with the highest heat transfer and the least pressure loss. The trade-off point satisfies both objective functions of pressure loss and heat transfer acquired by the mapping technique.

5. Based on the optimizing results, the best thermal-hydraulic performance for a flattened tube with porous layers is obtained with H=*4* mm, H_p=*0.75*, ε =*0.3*, Q=*0.0073* m^3/h and q''=*10000* W/m^2.

6. It was indicated that the acquired Pareto front can differentiate the best boundary of the experimental data regarding the highest quantity of heat transfer coefficient and minimum of the pressure drop confirming the validity of the multi-objective optimizing method provided in this work.

NOMENCLATURE

A_i	fuzzy sets
AC_i	actual value
ANFIS	Adaptive Nero Fuzzy Inference System
a_{sf}	Specific fluid-to-solid surface area
B_i	fuzzy sets

C_p	specific heat, J/(kg K)
C_f	Friction factor
d	particle diameter, m
D_h	hydraulic diameter, m
F	Inertia parameter
f_i	ANFIS system's output
H	Tube height
H_p	Porous layer thickness
h	heat transfer coefficient, W/(m^2 K)
hsf	fluid-to-solid heat transfer coefficient W/(m^2 K)
k	thermal conductivity, W/(m K)
k_{fe}	effective thermal conductivity of the fluid, W/m K
k_{se}	effective thermal conductivity of the solid, W/m K
K	permeability (m^2)
L	length of flat tube, m
$MRE\%$	mean relative error
MSE	mean squared error
Nu	Nusselt number
O_{ij}	ANFIS layers output
P	pressure, Pa
PR_i	ANFIS predicted output
p_i	linear output
Pr	Prandtl number
Q	Entrance flow rate
q''	heat flux, W/m^2
q_i	linear output
Re	Reynolds number
$RE\%$	relative error
R^2	correlation coefficient
r_i	linear output
T	temperature, K
V	velocity, m/s
W	width of flat tube, mm
W_i	ANFIS normalized firing strength
Z	axial distance from inlet, m

Greek symbols

α	thermal diffusivity (=k/ ρ C_p) (m^2/s)
ε	porosity
ρ	density, kg/m3
μ	dynamic viscosity (kg/ m.s)
τ_w	wall shear stress (Pa)

Subscripts

0	Plain tube
e	effective
f	fluid
i	inlet
$interface$	interface between the porous medium and the clear region
p	porous
s	solid
w	wall
x	X direction
y	Y direction
z	Z direction

REFERENCES

[1] B. Alazmi, K. Vafai, Constant wall heat flux boundary conditions in porous media under local thermal non-equilibrium conditions, International Journal of Heat and Mass Transfer 45 (2002) 3071–3087.

[2] A.A. Mohamad, Heat transfer enhancements in heat exchangers fitted with porous media Part I: constant wall temperature, International Journal of Thermal Sciences 42 (2003) 385–395.

[3] B.I. Pavel, A.A. Mohamad, An experimental and numerical study on heat transfer enhancement for gas heat exchangers fitted with porous media, International Journal of Heat and Mass Transfer 47 (2004) 4939–4952.

[4] H. Shokouhmand, F. Jam, M.R. Salimpour, Simulation of laminar flow and convective heat transfer in conduits filled with porous media using Lattice Boltzmann Method, International Communications in Heat and Mass Transfer 36 (2009) 378-384.

[5] H. Shokouhmand, F. Jam, M.R. Salimpour, The effect of porous insert position on the enhanced heat transfer in partially filled channels, International Communications in Heat and Mass Transfer 38 (2011) 1162–1167.

[6] K. Yang, K. Vafai, Analysis of heat flux bifurcation inside porous media incorporating inertial and dispersion effects e an exact solution, International Journal of Heat and Mass Transfer 54 (2011) 5286-5297.

[7] K. Yang, K. Vafai, Restrictions on the validity of the thermal conditions at the porous-fluid interfaced an exact solution, Journal of Heat Transfer 133 (2011) 112601.

[8] T.Z. Ming, Y. Zheng, J. Liu, C. Liu, W. Liu, S.Y. Huang, Heat transfer enhancement by filling metal porous medium in central area of tubes, Journal of the Energy Institute 83 (2010) 17-24.

[9] R. Vajjha, D. Das, P. Namburu, Numerical study of fluid dynamic and heat transfer performance of Al2O3 and CuO nanofluids in the flat tubes of a radiator, International Journal of Heat and Fluid Flow 31 (2010) 613–621.

[10] P. Razi, M. Akhavan-Behabadi, M. Saeedinia, Pressure drop and thermal characteristics of CuO-base oil nanofluid laminar flow in flattened tubes under constant heat flux, International Communications in Heat and Mass Transfer 38 (2011) 964–971.

[11] H. Safikhani, A. Abbassi, Effects of tube flattening on the fluid dynamic and heat transfer performance of nanofluids, Advanced Powder Technology 25 (2014) 1132–1141.

[12] H. Safikhani, A. Abbassi, A. Khalkhali, M. Kalteh, Multi-objective optimization of nanofluid flow in flat tubes using CFD, Artificial Neural Networks and genetic algorithms, Advanced Powder Technology 25 (2014) 1608–1617.

[13] J.S.R. Jang, R. May, ANFIS: Adaptive network based fuzzy inference systems, IEEE Transactions on Systems, Man, and Cybernetics, 23 (1993) 665–685.

[14] H. Esen, M. Inalli, A. Sengur, M. Esen, Modelling a ground-coupled heat pump system using adaptive neuro-fuzzy inference system, International Journal of Refrigeration 31 (2007) 65-74.

[15] H. Esen, M. Inalli, A. Sengur, M. Esen, Artificial neural networks and adaptive neuro fuzzy assessments for ground-coupled heat pump system, Energy and Buildings 40 (2008) 1074-1083.

[16] H. Esen, M. Inalli, ANN and ANFIS models for performance evaluation of a vertical ground source heat pump system, Expert Systems with Applications 37 (2010) 8134-8147.

[17] W. Yaïci, E. Entchev, Adaptive Neuro-Fuzzy Inference System modelling for performance prediction of solar thermal energy system, Renewable Energy 86 (2016) 302-315.

[18] K. Ermis, A. Erek, I. Dincer, Heat transfer analysis of phase change process in a finned-tube thermal energy storage system using artificial neural network, International Journal of Heat and Mass Transfer 50 (2007) 3163-3175.
[19] H.M. Ertunca, M. Hosoz, Comparative analysis of an evaporative condenser using artificial neural network and adaptive neuro-fuzzy inference system, International Journal of Refrigeration 31 (2008) 1426-1436.
[20] M. Hosoz, H.M. Ertunc, H. Bulgurcu, An adaptive neuro-fuzzy inference system model for predicting the performance of a refrigeration system with a cooling tower, Expert Systems with Applications 38 (2011) 14148-14155.
[21] T.R. Kiran, S.P.S. Rajput, An effectiveness model for an indirect evaporative cooling (IEC) system: comparison of artificial neural networks (ANN), adaptive neuro-fuzzy inference system (ANFIS) and fuzzy inference system (FIS) approach, Applied Soft Computing 11 (2011) 3525-3533.
[22] A.S., Sahin, Performance analysis of single-stage refrigeration system with internal heat exchanger using neural network and neuro-fuzzy, Renewable Energy 31 (2011) 2747-2752.
[23] T.H. Lee, J.Y. Yun, J.S. Lee, J.J. Park, K.S. Lee, Determination of airside heat transfer coefficient on wire-on tube type heat exchanger, International Journal of Heat and Mass Transfer 44 (2001) 1767-1776.
[24] Y. Varol, E. Avci, A. Koca, H.F. Oztop, Prediction of flow fields and temperature distributions due to natural convection in a triangular enclosure using Adaptive-Network-Based Fuzzy Inference System (ANFIS) and Artificial Neural Network (ANN), International Communications in Heat and Mass Transfer 34 (2007) 887-896.
[25] Y. Varol, A. Koca, H.F. Oztop, E. Avci, Analysis of adaptive-network-based fuzzy inference system (ANFIS) to estimate buoyancy-induced flow field in partially heated triangular enclosures, Expert Systems with Applications 35 (2008) 1989-1997.
[26] M. Hayati, A. Rezaei, M. Seifi, Prediction of the heat transfer rate of a single layer wire-on-tube type heat exchanger using ANFIS. Short Communication, International Journal of Refrigeration 32 (2009) 1914-1917.
[27] E. Rezaei, A.M. Karami, T. Yousefi, S. Mahmoudinezhad, Modeling the free convection heat transfer in a partitioned cavity using ANFIS, International Communications in Heat and Mass Transfer 39 (2012) 470-475.
[28] T.A. Tahseen, M. Ishak, M.M. Rahman, Performance predictions of laminar heat transfer and pressure drop in an in-line flat tube bundle using an adaptive neuro-fuzzy inference system (ANFIS) model, International Communications in Heat and Mass Transfer 50 (2014) 85-97.
[29] S. Soyguder, H. Alli, Predicting of fan speed for energy saving in HVAC system based on adaptive network based fuzzy inference system, Expert Systems with Applications 36 (2009) 8631-8638.
[30] A. Swain, M. Kumar das, Prediction of Heat Transfer Coefficient in Flow Boiling over Tube Bundles Using ANFIS, Heat Transfer Engineering 37 (2016) 443-455.
[31] A. Hasiloglu, M. Yilmaz, O. Comakli, İ. Ekmekci, Adaptive neuro-fuzzy modeling of transient heat transfer in circular duct air flow, International Journal of Thermal Sciences 43 (2004) 1075-1090.
[32] M. Mehrabi, S.M. Pesteei, T.G. Pashaee, Modeling of heat transfer and fluid flow characteristics of helicoidal double-pipe heat exchangers using Adaptive Neuro-Fuzzy Inference System (ANFIS), International Communications in Heat and Mass Transfer 38 (2011) 525–532.
[33] S. Wang, J. Xiao, J. Wang, G. Jian, J. Wen, Z. Zhang, Application of response surface method and multi-objective genetic algorithm to conFiguration optimization of Shell-and-tube heat exchanger with fold helical baffles, Applied Thermal Engineering. 129 (2018) 512-520.
[34] H. Liu, H. Zhang, F. Yang, X. Hou, F. Yu, S. Song, Multi-objective optimization of fin-and-tube evaporator for a diesel engine organic Rankine cycle (ORC) combined system using particle swarm optimization algorithm, Energy Conversion and Management 151 (2017) 147–157.
[35] N. Zheng, P. Liu, X. Wang, F. Shan, Z. Liu, W. Liu, Numerical simulation and optimization of heat transfer enhancement in a heat exchanger tube fitted with vortex rod inserts, Applied Thermal Engineering 123 (2017) 471-484.
[36] S. Wang, J. Xiao, J. Wang, J. Guanping, W. Jian, Zh. Zaoxiao, Configuration optimization of shell-and-tube heat exchangers with helical baffles using multi-objective genetic algorithm based on fluid-structure interaction, International Communications in Heat and Mass Transfer 85 (2017) 62–69.
[37] A.G. Ivakhnenko, Polynomial theory of complex systems, IEEE Transactions on Systems, Man, and Cybernetics, SMC-1 (1971) 364-378.
[38] H. Safikhani, M.A. Akhavan-Behabadi, N. Nariman-Zadeh, M.J. Mahmood Abadi, Modeling and multi-objective optimization of square cyclones using CFD and neural networks, Chemical Engineering Research and Design 89 (2011) 301–309.
[39] H. Safikhani, Modeling and multi-objective Pareto optimization of new cyclone separators using CFD, ANNs and NSGA II algorithm, Advanced Powder Technology 27 (2016) 2277-2284.
[40] M.D. Damavandi, M. Forouzanmehr, H. Safikhani, Modeling and Pareto based multi-objective optimization of wavy fin-and-elliptical tube heat exchangers using CFD and NSGA-II algorithm, Applied Thermal Engineering 111 (2017) 325–339.
[41] M.D. Damavandi, S.M. Mousavi, H. Safikhani, Pareto optimal design of swirl cooling chambers with tangential injection using CFD, GMDH-type of ANN and NSGA-II algorithm, International Journal of Thermal Sciences 122 (2017) 102-114.
[42] K. Deb, A. Pratap, S. Agarwal, T. Meyarivan, A fast and elitist multiobjective genetic algorithm: NSGA-II, IEEE Transactions on Evolutionary Computation, 6 (2002) 182-197.
[43] H. Safikhani, A. Hajiloo, M.A. Ranjbar, Modeling and multi-objective optimization of cyclone separators using CFD and genetic algorithms, Computers & Chemical Engineering 35 (2011) 1064–1071.
[44] D.A. Nield, A. Bejan, Convection in Porous Media, Springer, New York, 2013.
[45] Y. Mahmoudi, N. Karimi, Numerical investigation of heat transfer enhancement in a pipe partially filled with a porous material under local thermal non-equilibrium condition, International Journal of Heat and Mass Transfer 68 (2014) 161–173.
[46] T. Takagi, M. Sugeno, Fuzzy identification of systems and its application to modeling and control, IEEE Transactions on Systems, Man, and Cybernetics, 15 (1985) 116–132.
[47] J.S.R. Jang, C.T. Sun, E. Mizutani, Neuro-Fuzzy and Soft Computing, A Computational Approach to Learning and Machine Intelligence, Prentice Hall, NJ, USA, 1997.
[48] L.A. Zadeh, Fuzzy sets, Information and Control 8 (1965) 338-353.
[49] C.D. Montgomery, Design and Analysis Experiments, John Wiley & Son, 1991.
[50] G. Jekabsons, J. Lavendels, A comparison of heuristic methods for polynomial regression model induction, Mathematical Modelling and Analysis 13 (2008) 17–27.
[51] S.J. Farlow, Self-organizing methods in modeling: GMDH type algorithms, CRC Press, 1984.

HOW TO CITE THIS ARTICLE

E. Rezaei, A. Abbassi. Computational fluid dynamics modeling and multi-objective optimization of flat tubes partially filled with a porous layer using ANFIS, GMDH, and NSGA II approaches. AUT J. Mech Eng., 4(4) (2020) 449-464.

DOI: 10.22060/ajme.2020.16836.5836